Excitonic singlet-triplet ratios in molecular and polymeric organic materials

M. Segal and M. A. Baldo*

Department of Electrical Engineering and Computer Science, Massachusetts Institute of Technology, 77 Massachusetts Av., Cambridge, Massachusetts 02139, USA

R. J. Holmes and S. R. Forrest

Center for Photonics and Optoelectronic Materials (POEM), Department of Electrical Engineering and the Princeton Materials Institute, Princeton University, Princeton, New Jersey 08544, USA

Z. G. Soos

Department of Chemistry, Princeton University, Princeton, New Jersey 08544, USA

A simple technique employing reverse bias measurements of photoluminescent efficiency is described to determine the excitonic singlet-triplet formation statistics of electroluminescent organic thin films. Using this method, the singlet fractions in thin films of two organic emissive materials commonly used in organic light emitting devices, tris(8-hydroxyquinoline) aluminum (Alq$_3$) and poly[2-methoxy-5-(2-ethylhexyloxy)-1,4-phenylenevinylene] (MEH-PPV), are found to be $(20\pm1)\%$ and $(20\pm4)\%$, respectively. Results are confirmed using a sensitive synchronous detection scheme. We discuss other measurements and the current understanding of exciton formation statistics in polymeric and small molecular weight organic electroluminescent materials.

I. INTRODUCTION

Understanding the mechanisms underlying exciton formation from injected charge in organic semiconductors is an outstanding challenge in the field of organic electroluminescence. Indeed, the ratio of singlets to triplets represents an important manifestation of the dynamics of exciton formation,[1–6] that is critical to the efficiency of fluorescent organic light emitting devices. From simple statistical considerations, the ratio of singlets to triplets in the spin-degeneracy limit is 1:3. Phosphorescent molecular organic light emitting devices (OLED's) exhibit efficiencies approximately four times that of molecular OLED's that fluoresce from singlets alone, consistent with the spin-degeneracy limit.[7] But other experiments suggest that exciton statistics in *polymeric* semiconductors may favor luminescent singlets over nonemissive triplet excitons.[1,3–6] If so, fluorescent polymers may possess intrinsically higher electroluminescent efficiencies than fluorescent small molecules, although to date this difference has not been consistently observed.

Excited species comprising an electron and a hole are typically modeled in organic semiconductors as two-electron systems, with one electron in a partially filled lowest unoccupied molecular orbital (LUMO), and the other in a partially filled highest occupied molecular orbital (HOMO). The total spin S of the two-electron combination is either $S=0$ (singlet) or 1 (triplet). In organic molecules, the triplet excited state is typically lower in energy than the singlet excited state by $2K$, where $K\approx0.5$ eV is the exchange integral involving the HOMO and LUMO. Unlike the long-range Coulomb interaction, K depends on the overlap of the electron (e) and hole (h) wave functions and hence decreases exponentially with e-h separation, r. The exchange splitting $2K$ between singlet and triplet excitons in conjugated polymers is ≈1.0 eV,[8] comparable to molecular values.

The photophysics of organic molecules[9] deals with intramolecular processes. In addition, we must consider various intermolecular processes[10] in organic semiconductors when, for example, the electron and hole are injected into the film from opposing contacts. Figure 1 presents a general picture for exciton formation in organic semiconductors with r as the reaction coordinate for both intramolecular and intermolecular excited species. The model classifies a continuum of possible excited species into Frenkel excitons, charge-transfer (CT) states, and extended polaron pairs. Excited states are generated either by optical excitation or through the combination of positive and negative injected charge. Optical ex-
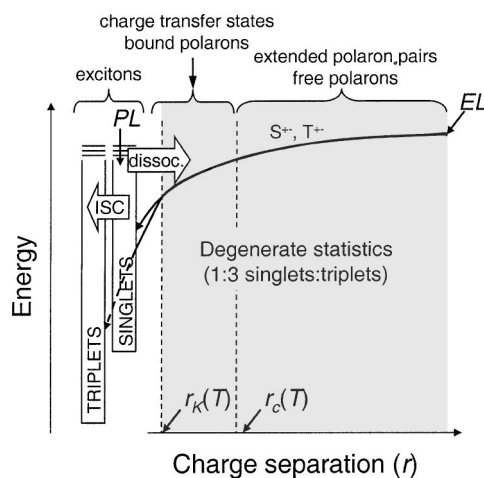

FIG. 1. Injected electrons and holes in organic semiconductors may form either singlet or triplet excitons. At large charge separations, singlet and triplet pair states are degenerate, and it is assumed that there is one singlet pair for every three triplet pairs. Once bound by Coulombic interactions, the formation of excitons is mediated by charge-transfer (CT) states.
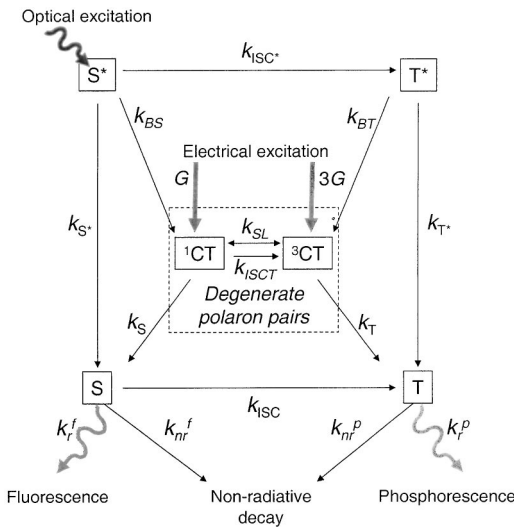
FIG. 2. A rate model for electrical and photoexcitation of polymers with charge-transfer (CT) states. Knowledge of the fraction of excited singlet states S^* that decay into CT states is essential in the determination of the singlet fraction χ_S.

citation predominantly results in singlet Frenkel excitons, since these species have the largest oscillator strengths. On the other hand, electrical excitation and the injection of opposite charges initially form extended polaron pairs, which can collapse to form CT states and excitons as described by Fig. 1. Each species can be either singlet or triplet.

Frenkel excitons are localized, with the bound electron and hole on the same molecule ($r < 10$ Å). Intersystem crossing (ISC) from singlet to triplet provides a mechanism for indirect optical excitation of triplets. At large $r > 100$ Å we have positive and negative polarons, or radical ions, whose $S = \frac{1}{2}$ spins are not correlated; thus, $S = 0$ and 1 are degenerate and $K = 0$. The capture radius r_c at which $kT = q^2/r_c$ can be used to define independent polarons, where, q is the electronic charge, k is Boltzmann's constant, and T is the temperature. In contrast, CT states occur from $r < r_c$ down to nearest-neighbor ion pairs. Singlet and triplet CT states are usually considered to be degenerate due to the short-range nature of K, although this may not hold strictly for charge transfer between adjacent molecular sites. We define r_K in Fig. 1 as the *e-h* separation at which singlet-triplet splittings become small, and weak perturbations can mix the states. It is expected that r_K is on the order of molecular dimensions, i.e., $r_K \approx 10$ Å.

The energy range in Fig. 1 contains a continuum of Frenkel and CT states that in principle have different photophysical parameters. In polymers, as in molecules,[9] we focus on a few discrete states depicted in Fig. 2. Optical excitation generates high-energy singlet excitons S^* that may relax to the lowest excited singlet S with rate k_{S*}; S^* can also cross over to an excited triplet T^* with rate k_{ISC*} or charge separate to a lower-energy CT state with rate k_{BS}. Similarly, the excited triplet can charge separate with rate k_{BT} or decay to a relaxed triplet with rate k_{T*}. The rates k_S and k_T are the formation rates of singlet and triplet excitons, respectively, from *degenerate* CT states. Electrical excitation then pro-

ceeds through degenerate polaron pairs and degenerate CT states that ultimately collapse to excitons. The CT states included in Fig. 2 have $r > r_K$, and together with extended polaron pairs, are classified simply as "degenerate polaron pairs." CT states with $r < r_K$ are assumed to relax directly to their respective singlet and triplet Frenkel excitons and are not explicitly shown. The rates k_S and k_T are so defined because the formation rates for singlet and triplet excitons from *nondegenerate* CT states will have little effect on the ratio of singlet to triplet excitons formed. The rates k_S and k_T are central to interpreting recent studies of polymer emission.[1,3–6]

Singlet and triplet polaron pairs, and CT states with $r > r_K$, are typically mixed by spin-lattice interactions, by dipolar or hyperfine fields, and by spin-orbit interactions that are particularly small for π electrons.[11] The mixing rate k_{SL} represents spin-lattice mixing between degenerate singlet and triplet CT states, which is expected to dominate other mixing processes. In electroluminescence, injected charges will have randomized spin states in any case. Thus polaron pairs are expected to be formed in the ratio of 1:3 singlets to triplets.

Once the singlet and triplet states are split at $r < r_K$, mixing effectively ceases under small perturbations, so that there is no mixing rate between singlet and triplet excitons in Fig. 2. However, intersystem crossing from S to T at lower energy is possible for both excitons and CT states, with rates k_{ISC} and k_{ISCT}, respectively. Although typically small, k_{ISC} and k_{ISCT} may be significantly enhanced in the presence of heavy atoms such as Pt or Ir, which greatly increase the strength of spin-orbit coupling, and hence the population of triplet excitons. Intersystem crossing from high-energy S^* to T^* may proceed at different rates than from the lowest S to T. Indeed, high-energy photoexcitation of anthracene has been observed to result in a singlet-to-triplet ratio of 1:1, while low-energy photoexcitation results in a 1:3 ratio.[12]

It is apparent therefore that an accurate determination of the singlet-to-triplet ratio is essential to understanding the physical mechanisms leading to electroluminescence in organic thin films. Yet while many authors have reported this formation ratio, there remains disagreement as to its value, particularly in technologically interesting luminescent polymeric semiconductors. Several previous studies of exciton formation have been based on a comparison of the electroluminescent (EL) and photoluminescent (PL) efficiencies of a particular material.[1–3,5] In this work, a simple technique is described that avoids many systematic errors that may arise in comparative measurements. As a demonstration, the two archetypal luminescent compounds, tris(8-hydroxyquinoline) aluminum (Alq$_3$) and poly[2-methoxy-5-(2-ethylhexyloxy)-1,4-phenylenevinylene] (MEH-PPV), are analyzed and found to possess singlet fractions of $(20 \pm 1)\%$ and $(20 \pm 4)\%$, respectively.

Section II of this paper describes the theory of reverse bias measurements of PL efficiencies, and Sec. III describes the experimental details of the measurement of singlet fractions. Section IV presents the measured PL efficiencies for Alq$_3$ and MEH-PPV OLED's. In Sec. V the singlet fractions are determined for Alq$_3$ and MEH-PPV, and a model for

EL-specific losses is proposed to place an upper bound on the singlet ratio in these materials. Different measurement techniques are compared in Sec. VI, and possible material dependencies in the singlet fraction are discussed in the conclusion, Sec. VII.

II. THEORY OF REVERSE BIAS MEASUREMENT OF PL EFFICIENCY

Exciton formation statistics determine the external quantum efficiency of electroluminescence in an OLED, η_{EL}:[3]

$$\eta_{EL} = \chi_S \gamma \eta_C \eta_{PL}, \tag{1}$$

where the fraction of excitons formed as singlets is χ_S, η_{PL} is the intrinsic PL efficiency, the light output coupling fraction η_C is the fraction of emitted photons captured by the detector, and $\gamma \leq 1$ measures losses present in EL but not in PL.[3]

The product $\eta_C \eta_{PL}$ is determined by optically exciting the luminescent organic film within an OLED placed under reverse electrical bias. The electric field dissociates some excitons into charges,[10,13,14] reducing the PL and generating photocurrent, thereby providing an accurate measurement of the number of excitons dissociated. As shown below, the ratio of the change in PL to the photocurrent gives $\eta_C \eta_{PL}$. Because this technique also allows for the measurement of η_{EL} in the same experimental geometry used to measure η_{PL} by applying forward bias to the luminescent film and injecting charges, it is not necessary to explicitly measure η_C, avoiding uncertainties commonly associated with this measurement.

The PL power (P_{PL}) emitted by the optically excited film is given by

$$P_{PL} = \eta_C h \nu \frac{k_R}{k_R + k_{NR} + k_Q} \phi, \tag{2}$$

where ϕ is the photon flux from the excitation source absorbed within the film, k_R is the radiative exciton recombination rate, k_{NR} is the nonradiative decay rate, k_Q is the rate of electric field-induced quenching, h is Planck's constant, and ν is the frequency of the radiated photons. For weak field-induced quenching [i.e., $k_Q \ll (k_R + k_{NR})$], the drop in PL may be expressed in terms of the PL efficiency in the absence of an applied field, i.e., $\eta_{PL} = k_R / (k_R + k_{NR})$, to obtain

$$\Delta P_{PL} = P_{PL}(k_Q) - P_{PL}(k_Q = 0) \approx -h \nu \eta_C \eta_{PL} \frac{k_Q}{k_R + k_{NR}} \phi. \tag{3}$$

In all devices used in this study, the field-induced PL quenching satisfies $k_Q \ll (k_R + k_{NR})$. The photocurrent resulting from field-induced dissociation of excitons is

$$I_{ph} = q \frac{k_Q}{k_R + k_{NR} + k_Q} \phi \tag{4}$$

where q is the electronic charge. Assuming that $k_Q \ll (k_R + k_{NR})$, Eqs. (3) and (4) give

$$\eta_C \eta_{PL} = -\frac{q}{h \nu} \frac{\Delta P_{PL}}{I_{ph}}. \tag{5}$$

Since the EL power, P_{EL}, at an injected current, I_{inj}, is given by $P_{EL} = q I_{inj} h \nu \eta_{EL}$, and using Eq. (1), we can write

$$\chi_S \gamma = \frac{\eta_{EL}}{\eta_C \eta_{PL}} = \frac{P_{EL}}{I_{inj}} \bigg/ \frac{-\Delta P_{PL}}{I_{ph}}. \tag{6}$$

Thus spin statistics are obtained from η_{EL} and the ratio of differential photoluminescence ΔP_{PL} to photocurrent I_{ph}. Simultaneous measurements of current and differential photoluminescence are readily performed in most OLED's under steady-state reverse bias.

The reverse bias current has two components that must be detected separately, photocurrent, I_{ph} and leakage current, I_{leak}. In addition, fluctuations in optical pump intensity may introduce noise into measurements of ΔP_{PL}. Two-tone synchronous detection can be used to discriminate between I_{ph} and I_{leak} and detect only that portion of ΔP_{PL} due to electric-field modulation. The reverse bias and optical pump intensity are modulated at angular frequencies ω_B and ω_L, respectively, and I_{ph} and ΔP_{PL} are detected at ω_L and ω_B, respectively. Synchronous detection is employed here to confirm results taken with unmodulated (dc) excitations, and is essential for measuring devices where leakage current may exceed photocurrent, such as for the MEH-PPV OLED's in this study. Synchronous detection may also be used as a stand-alone technique. The theory of two-tone synchronous detection of photoluminescent efficiency is described in the Appendix.

We note that charge generation during optical excitation may lead to underestimates of the PL efficiency and corresponding overestimates of χ_S; see Sec. IV B. Exciton dissociation is enhanced when the film is excited at energies significantly above the absorption edge,[15] and consequently, in this work, the optical pump wavelength is selected as close as possible to the HOMO-LUMO gap. Because CT states can also be dissociated into photocurrent under reverse bias, the reverse bias technique may be a sensitive probe for charge generation, providing an inherent guard against underestimating PL efficiency. Indeed, lower, nonlinear, $\Delta P_{PL}/I_{ph}$ slopes were measured when higher-energy optical pumps were used.[16] Since knowledge of the outcoupling efficiency is not required in our method, the reverse bias technique offers advantages over conventional, absolute measurements of PL efficiency in determinations of the singlet-triplet formation statistics.

III. EXPERIMENTAL TECHNIQUE

To compare the EL and PL efficiencies in small molecular weight and polymeric materials, two types of OLED's were fabricated. Polymeric OLED's used an emissive and hole-transporting layer (HTL) layer of the polymer MEH-PPV,[17] and small molecular weight materials were studied using an emissive layer of Alq_3. All devices were fabricated on cleaned and UV-ozone treated glass substrates pre-coated with an indium tin oxide (ITO) anode with a sheet resistance of $\approx 20 \ \Omega/sq$. To enhance hole injection from
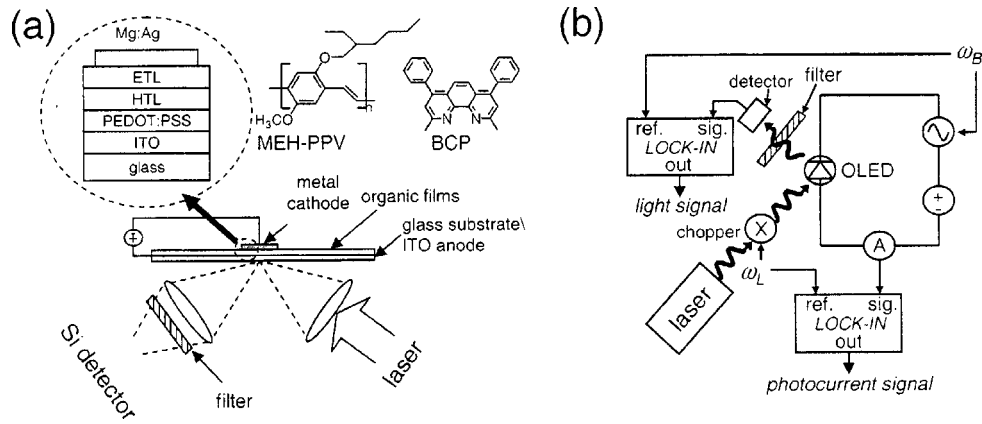
FIG. 3. (a) The experimental setup of the dc PL efficiency measurement. PL from an optically excited OLED is focused onto a calibrated silicon detector. An optical filter is used to remove the pump light from the collected light. The OLED is placed under a varying reverse bias that partially quenches the PL. The out-coupled PL efficiency is obtained by comparing the change in PL (ΔP_{PL}) to the photocurrent. Inset: A cross section of the OLED's. Charges and excitons within the organic layer under test are confined by a heterostructure employing bathocuproine (BCP) as the electron transport (ETL) and hole blocking layer. The semiconducting polymer MEH-PPV was used as a hole transport layer (HTL). (b) The experimental setup of the synchronous PL efficiency measurement. Here the photocurrent and out-coupled PL are detected by locking the photocurrent to the optical chopping frequency, and the PL to the modulation frequency of the reverse bias voltage. This scheme rejects leakage current, optical pump fluctuation, and detected light noise.

the anode, all devices used a thin layer of poly(3,4-ethylenedioxythiophene):poly(4-styrenesulphonate) (PEDOT:PSS). This layer was prepared by spin coating onto the ITO substrate followed by baking at $T \approx 120\,°C$ for at least 30 min in an oxygen-free environment. The polymer OLED's had an approximately 300-Å-thick layer of MEH-PPV spun cast onto the PEDOT:PSS layer from 3:7 tetrahydrofuran-toluene solvent, and baked in an oxygen-free environment at $T \approx 115\,°C$ for at least 10 h. The Alq$_3$ OLED's had a 500-Å-thick HTL composed of N,N'-diphenyl-N,N'-bis(3-methylphenyl)-$[1,1'$-biphenyl] 4,4$'$-diamine (TPD) deposited onto the PEDOT:PSS layer, followed by a 200-Å-thick light-emitting layer of Alq$_3$. The TPD and Alq$_3$ layers were deposited by high-vacuum (10^{-6} Torr) thermal evaporation, as were all layers comprised of small molecules. Both types of devices contained an electron transport layer (ETL) 2,9-dimethyl-4,7-diphenyl-1,10-phenanthroline (BCP), chosen because of its transparency to the optical pump beams at $\lambda = 405$ nm and at $\lambda = 532$ nm, and its efficient hole and exciton-blocking capability.[2] The thickness of the BCP layer was 500 Å in Alq$_3$ devices, and for reasons described in Sec. IV, 150 Å in the MEH-PPV devices. A shadow mask with 1-mm-diameter

openings was used to define the cathode in all devices. The cathodes consisted of a layer of approximately 60:1 Mg:Ag followed by a Ag cap to protect against oxidation. Alq$_3$ devices had a 1000-Å-thick Mg:Ag layer and a 200-Å-thick Ag cap, whereas MEH-PPV devices had a 500-Å-thick Mg:Ag layer followed by a 500-Å-thick Ag cap.

The experimental setups for the dc and synchronous PL efficiency measurements are shown in Figs. 3(a) and (b), respectively. Two diode lasers were employed as optical sources, one with wavelength $\lambda = 405$ nm and another at $\lambda = 532$ nm. The lasers had continuous maximum output powers of 3.4 and 25 mW, respectively. A lens was used to focus the pump laser to an approximately 1-mm-diameter spot, aligned with the OLED cathode. Fluorescence was collected by a second lens, and was optically filtered to remove the pump wavelength before being focused onto a silicon detector. The collection optics were calibrated by comparing the EL efficiency in this geometry to that measured by placing the OLED directly onto the surface of a large-area silicon detector.[7] Although this did not affect measurement of the singlet fraction, measurement of the total light emitted in the forward direction enables calculation of the out-coupling efficiency η_C. In the two-tone synchronous measurement
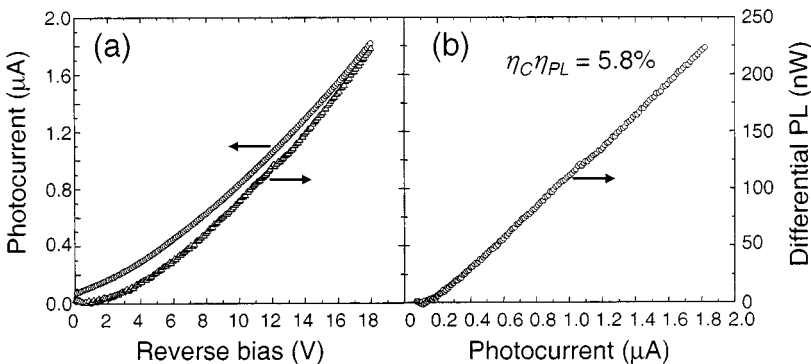

FIG. 4. (a) Magnitude of change in PL, ΔP_{PL}, and the corresponding photocurrent I_{ph} in Alq$_3$ as a function of reverse bias. (b) The relation between ΔP_{PL} and I_{ph}, given by Eq. (8), gives the out-coupled PL efficiency $\eta_C \eta_{PL}$.
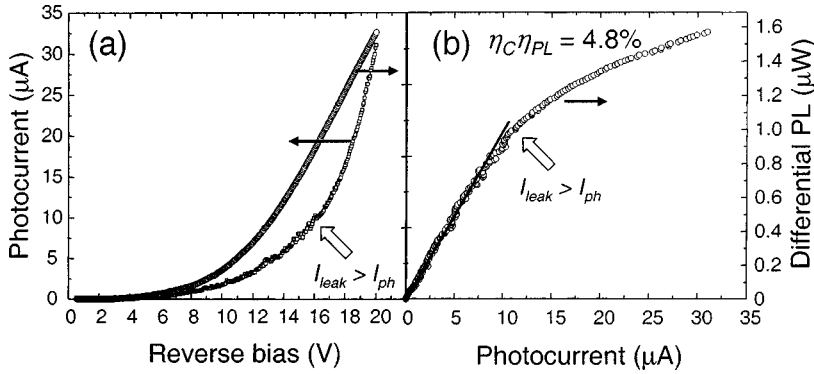
FIG. 5. (a) Magnitude of change in PL, ΔP_{PL}, and the corresponding photocurrent I_{ph} in MEH-PPV as a function of reverse bias. The "kink" in the photocurrent at $V \approx 16$ V corresponds to the voltage at which leakage current begins to dominate photocurrent. (b) The relation between ΔP_{PL} and I_{ph}, given by Eq. (8), gives the out-coupled PL efficiency $\eta_C \eta_{PL}$.

setup shown in Fig. 3(b), the laser light was mechanically chopped at angular frequency $\omega_L = 2\pi \cdot 390$ rad/s, yielding an approximately 50% duty cycle square wave. The reverse bias was modulated sinusoidally at angular frequency $\omega_B = 2\pi \cdot 510$ rad/s. Photocurrent and differential PL were detected using two lock-in amplifiers. Each measurement at a specific reverse bias voltage was averaged for 30 s. Except for low temperature measurements, which were performed under vacuum, all devices were measured in air.

IV. PHOTOLUMINESCENCE EFFICIENCY MEASUREMENTS

Figure 4(a) shows the reverse bias photocurrent I_{ph} and the magnitude of the electric-field-induced change in PL, ΔP_{PL}, in an Alq$_3$-OLED measured using the dc technique. All Alq$_3$ devices were excited at $\lambda = 405$ nm, the edge of the absorption band of Alq$_3$. The resultant out-coupled PL efficiency is shown in Fig. 4(b). A weighted sum of several measurements yields $\eta_C \eta_{PL} = (5.9 \pm 0.1)\%$ for Alq$_3$. At zero reverse bias, the devices exhibit weak photovoltaic action leading to a slight offset in the photocurrent that does not affect the PL efficiency measurement. The PL efficiency of Alq$_3$ has been previously measured to be $\eta_{PL} = (27 \pm 5)\%$,[18,19] yielding an out-coupling fraction of $\eta_C = (24 \pm 4)\%$. Due to weak microcavity effects, η_C is expected to be dependent on the position of the luminescent region within the device structure.[20] The PL efficiency of Alq$_3$ measured using the dc technique was confirmed with a synchronous measurement.

Similarly, dc measurements of I_{ph} and ΔP_{PL} in MEH-PPV

are shown in Fig. 5(a) for optical excitation at the absorption edge of MEH-PPV, at $\lambda = 532$ nm. The resultant out-coupled PL efficiency is shown in Fig. 5(b). Using Eq. (5), the slope of the linear regime at small I_{ph} yields $\eta_C \eta_{PL} = (4.8 \pm 0.1)\%$ for MEH-PPV. The PL efficiency of MEH-PPV was previously measured[21] to be $\eta_{PL} = 10-15\%$, yielding an out-coupling fraction of $\eta_C = 31-49\%$. We note that this is consistent with reports that solution processing of polymers may preferentially align radiative dipoles within the polymeric chains parallel to the reflective cathode, enhancing the out-coupling fraction relative to that of randomly oriented vacuum-deposited small molecular weight materials.[3]

The kink in the photocurrent characteristic in Fig. 5(a) (marked by the arrow) denotes the boundary between regions of markedly different noise behavior, and corresponds to the photocurrent at which the PL characteristic in Fig. 5(b) becomes nonlinear. These effects are interpreted to be the result of the reverse bias current being dominated by I_{ph} below the kink, and I_{leak} above it. Reverse bias leakage currents in MEH-PPV OLED's were often comparable to photocurrents and were unstable and inconsistent in repeated measurements. Consequently, synchronous detection was required to confirm MEH-PPV PL efficiencies measured using the dc technique.

Synchronous measurements of I_{ph} and ΔP_{PL} are shown in Fig. 6(a) for MEH-PPV, again for an excitation wavelength of $\lambda = 532$ nm. The out-coupled PL efficiency is $\eta_C \eta_{PL} = (4.8 \pm 0.2)\%$, in agreement with the dc result; see Fig. 5(b). Data points and error bars (both vertical and horizontal) represent the mean and standard deviation, respectively, of data collected at each reverse bias voltage. The linearity of
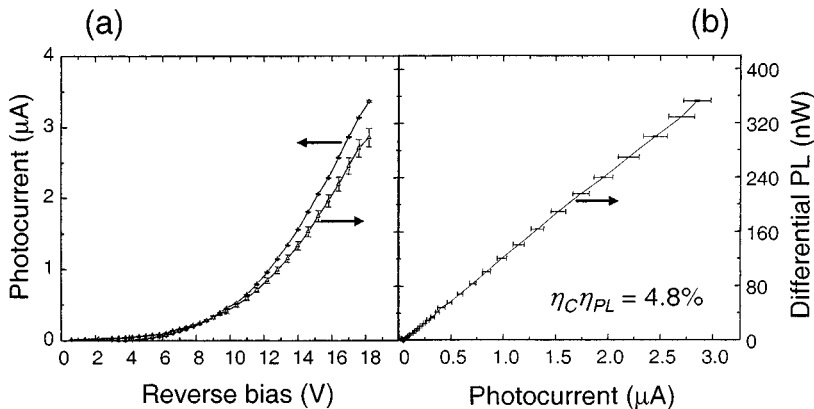

FIG. 6. (a) Synchronously-detected ΔP_{PL} magnitude and the corresponding photocurrent I_{ph} in MEH-PPV as a function of reverse bias. (b) The relationship between ΔP_{PL} and I_{ph}, in Eq. (8), gives the synchronously detected out-coupled PL efficiency $\eta_C \eta_{PL}$.
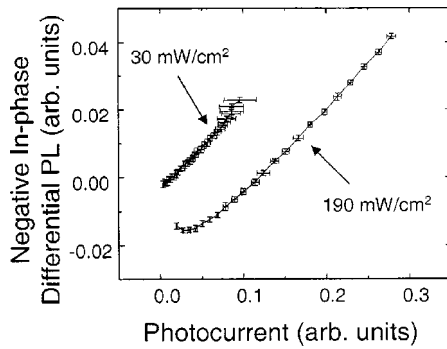
FIG. 7. The synchronously detected PL efficiency of Alq_3 is approximately independent of the optical pump intensity. The offset in ΔP_{PL} is due to increased charge generation within the film introduced by the higher intensity optical pump.
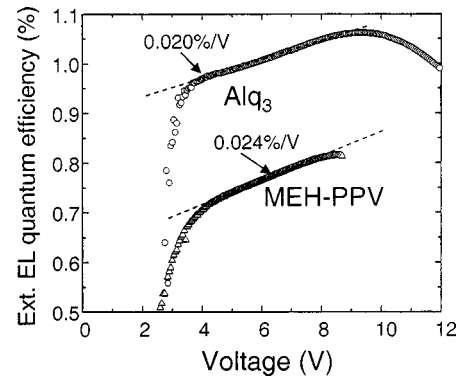

FIG. 8. The electroluminescent (EL) quantum efficiencies of an Alq_3 and an MEH-PPV OLED as functions of voltage, peaking at 1.06% and 0.81%, respectively. The linear dependence of the EL efficiency on voltage is consistent with the charge trap model described in Eq. (8).

the characteristic of Fig. 6(b) is especially notable, since both dc and synchronous measurements employ reverse bias voltages of up to 20 V. Thus the synchronous technique provides strong evidence that the discontinuity in slope observed in the dc PL measurement of Fig. 5(b) is due to leakage current.

Synchronous detection showed a negligible dependence on bias frequency. The phase of the ΔP_{PL} signal with respect to the voltage modulation changes rapidly at low photocurrent, from approximately $-180°$ to zero degrees. At low reverse bias then, ΔP_{PL} is *positive*, becoming negative at higher voltages. The increase in PL for low reverse bias is due to a reduction in singlet-polaron annihilation as photogenerated charge is detrapped by the electric field. At sufficiently high reverse bias, these charges are rapidly removed; and the increase in PL is overwhelmed by the electric-field-induced dissociation of excitons.

The effect of detrapping at low electric fields is more pronounced in the optical pump intensity dependence data shown in Fig. 7. There is no observed dependence in the slope of ΔP_{PL} versus I_{ph} above the zero crossing, consistent with η_{PL} independent of pump intensity. But the zero crossing is observed to shift in proportion to the pump intensity, confirming that increases in ΔP_{PL} at low bias (and hence low current) are due to reductions in the density of photogenerated charge.

Reverse bias measurements of the PL efficiency require complete collection of the photocurrent from dissociated excitons. Thus the OLED structure must be tailored to facilitate charge extraction. It was observed that the reverse bias ΔP_{PL} versus I_{ph} characteristics of MEH-PPV were nonlinear when thick films of BCP ($d > 150 \text{ Å}$) were used, most probably due to an energy barrier to electron transport across the MEH-PPV/BCP interface.[22,23] It has been proposed that thin BCP layers, although observed to efficiently block hole transport, assist in the extraction of electrons due to gap states in the material formed during deposition of the cathode that penetrate as far as $\approx 200 \text{ Å}$ from the cathode interface.[24] Indeed, highly efficient photovoltaic devices have been fabricated by using this method of charge extraction from the relatively deep lowest unoccupied molecular orbital of C_{60} at 4.6 eV.[24] With a 150-Å-thick BCP ETL, the yield of useful MEH-PPV devices (i.e., devices with linear reverse bias

characteristics) is close to 100%.

Accurate measurements of the PL efficiency also require that the technique be immune to the effects of geminate and nongeminate recombination involving charge from dissociated excitons, which may limit the extraction of photocurrent. The electric-field dependence of exciton dissociation under reverse bias is broadly consistent with the Onsager model.[10,13,14] However, due to the large electrostatic forces between geminate charges immediately following exciton dissociation, many geminate charge carriers will recombine before they can be extracted.[10] Use of the reverse bias technique requires that charges from singlet excitons dissociated by the applied electric field do not subsequently form nonemissive triplet excited states. The absence of an electric-field dependence of PL efficiency in reverse bias measurements demonstrates that geminate recombination occurs at times shorter than the spin dephasing time. The reverse bias technique is also observed to be unaffected by nongeminate recombination. Given a typical carrier mobility of $> 10^{-5} \text{ cm}^2/\text{V s}$, the density of minority carriers under reverse bias in both Alq_3 and MEH-PPV is small, $n < 10^{15} \text{ cm}^{-3}$. Low charge-carrier densities, and the high electric fields required to dissociate excitons and separate the resulting geminate charges, reduce the probability of nongeminate recombination, which increases with n^2. But most significantly, synchronous measurements demonstrate that the reverse bias PL efficiency is independent of leakage currents that frequently exceed 10 mA/cm^2, confirming the absence of nongeminate recombination in these devices.

V. ELECTROLUMINESCENCE EFFICIENCY MEASUREMENTS AND SINGLET FRACTIONS

The EL quantum efficiencies of the Alq_3 and MEH-PPV OLED's are shown in Fig. 8. When divided by the outcoupled PL efficiency, the EL efficiencies give an upper-bound estimate for the singlet fraction $\chi_S \gamma$ from Eq. (6) of $\chi_S \gamma = (18.0 \pm 0.3)\%$ for Alq_3 and $\chi_S \gamma = (17.0 \pm 0.7)\%$ for MEH-PPV. The EL-specific loss γ is thus required to obtain the singlet fraction χ_S. We summarize several loss mecha-
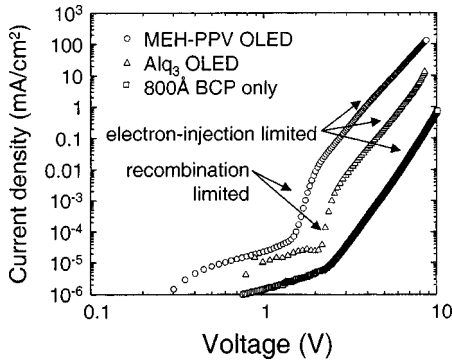
FIG. 9. The current-voltage (*I-V*) characteristics of an MEH-PPV and an Alq$_3$ OLED compared to electron-only transport in an 800-Å-thick film of BCP. At high biases, all devices are limited by electron injection into the BCP, but at voltages below the onset of exciton formation in the OLED's, the current density drops sharply, demonstrating that the OLED heterostructure forces unity charge balance in electroluminescence.

nisms and present a model for losses due to traps in both systems. EL-specific losses may be due to:

(i) Electron and hole currents may be unbalanced. This is considered unlikely in heterostructure devices because the currents are forcibly equalized using blocking layers such as BCP.[2] Figure 9 shows the current versus voltage (*I-V*) characteristics of both Alq$_3$ and MEH-PPV devices compared to a device consisting of only an 800-Å-thick BCP transport layer, sandwiched between PEDOT:PSS and a Mg:Ag cathode. Since BCP effectively blocks hole injection,[2] the similarity of the slopes of each of the characteristics for $V > 3$ V demonstrates that charge transport in each device is limited by electron injection.[25] At the onset of exciton formation in Alq$_3$ and MEH-PPV, the OLED's deviate from the BCP electron-only characteristic and demonstrate recombination-limited *I-V* characteristics, a clear indication of near unity charge balance in both heterostructure OLED's.

(ii) Microcavity effects[20,26] may affect PL and EL differently if the EL recombination zone is significantly narrower than the luminescent layer thickness. However, charges are confined within thin luminescent layers in this experiment, and hence microcavity effects are not expected to influence the results. To confirm this, devices were also fabricated with 250-Å-thick BCP layers, but no significant change in the singlet fraction χ_S was observed.

(iii) There may be significant polaron or field-induced quenching of singlet excitons, causing the EL quantum efficiency to decrease with increasing current density. The effects of such high-density phenomena may be minimized by extrapolating the quantum efficiency to its limit at low current.[27,28]

(iv) EL-specific losses may occur if electroluminescent excitons form preferentially at certain molecular sites such as charge traps.[2,29] There is no preference for exciton formation at these sites under photoexcitation. The luminescent efficiency of trap sites may be much lower than the average efficiency of excited molecules in the bulk film, especially if the traps are due to contamination. This process may result in an EL quantum efficiency η_{EL} that increases with applied
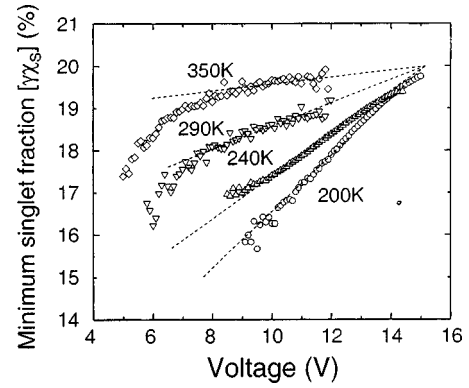

FIG. 10. The temperature dependence of the quantum efficiency of Alq$_3$ shows a significant increase in the slope of efficiency versus voltage as temperature decreases. This is attributed to exciton formation in trap states, resulting in EL-specific losses. The point at which the linear extrapolations intersect is V_{sat}.

voltage V and with temperature T since the traps can be saturated with charge, and charge detrapping is thermally activated. As evidence of the presence of low-luminescent-efficiency traps, it is noted that η_{EL} in guest-host films does not increase with V when the guest molecules act as *emissive* traps.[27,30,31] Instead, luminescent efficiencies of guest-host films typically decrease monotonically with increasing V due to exciton quenching by charges, while the efficiencies of neat luminescent materials usually peak with increasing excitation strength.[27,32]

Examination of the voltage and temperature dependencies of the EL efficiencies in Figs. 8 and 10, respectively, confirms the presence of EL-specific losses in both Alq$_3$- and MEH-PPV-based OLED's, i.e., $\gamma < 1$. We propose a simple model for traps that determines γ by extrapolating η_{EL} to its high current density limit. To explain the voltage and temperature dependencies of EL efficiency, we assume that each injected charge is either trapped, in which case it luminesces with quantum efficiency η_t, or it remains mobile and ultimately forms an exciton that luminesces with quantum efficiency η_f. We further assume that $\eta_f > \eta_t$. The probability of charge trapping is taken to be proportional to the fraction of trap sites remaining unfilled at voltage V, i.e., $(1 - V/V_{sat})$, where V_{sat} is defined as the voltage at which all the trap sites are saturated with space charge. Thus, η_{EL} is given by

$$\eta_{EL} = \eta_f \frac{V}{V_{sat}} + \eta_t \left(1 - \frac{V}{V_{sat}} \right), \quad V < V_{sat},$$

$$\eta_{EL} = \eta_f, \quad V > V_{sat}. \tag{7}$$

At V_{sat}, EL-specific losses due to traps vanish and $\gamma = 1$, $\eta_{EL} = \eta_f$. If V_{sat} is known, the linear dependence of η_{EL} on V can be extrapolated to determine η_f, the EL efficiency in the absence of EL specific losses, and hence the singlet fraction χ_S.

A worst-case value for V_{sat} can be calculated by recognizing that if a single trap site is present inside the radius of diffusion of an optically excited exciton, the exciton would
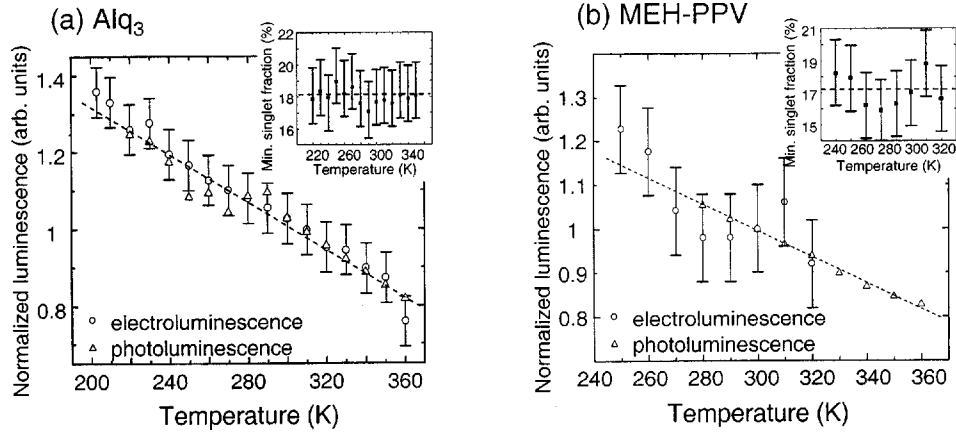
FIG. 11. (a) Photoluminescence (PL) and peak electroluminescence (EL) quantum efficiencies as functions of temperature in Alq_3. (b) The PL and peak EL quantum efficiencies as functions of temperature in MEH-PPV. In both Alq_3 and MEH-PPV, EL measured at large current densities ($J \approx 100$ mA/cm^2) tracks PL, demonstrating that the minimum singlet value $\gamma\chi_S$ is independent of temperature over the temperature range studied. Because $d(\gamma\chi_S)/dT \approx 0$, it is concluded that $\gamma \approx 1$. Insets: Inferred singlet fractions for Alq_3 and MEH-PPV.

diffuse to that trap site, eliminating any possible difference between EL and PL. This places an upper bound on trap density. The maximum area charge density necessary to fill all trap sites in the recombination zone is then

$$\sigma_{max} = t_{lum} \left/ \frac{4\pi}{3}L_D^3, \right. \tag{8}$$

where t_{lum} is the thickness of the luminescent layer and L_D is the exciton diffusion length. Then using $Q = CV$ gives the worst-case value of

$$V_{sat} = (q\sigma_{max}/\varepsilon)\left(t_{BCP} + \frac{t_{lum}}{2}\right), \tag{9}$$

where t_{BCP} is the thickness of the BCP layer and ε is the average of the dielectric constants of BCP and the luminescent material. Using $L_D = 40$ Å (typical for Förster transfer)[33] and the slopes $d\eta_{EL}/dV$ from Fig. 8 in Eq. (7), we find the worst-case $V_{sat} = 27$ V for Alq_3 and 20 V for MEH-PPV, corresponding to maximum values for η_f of 1.4% and 1.1%, respectively. This yields minimum values for γ of 0.76 and 0.74, leading to a maximum value of $\chi_S = (24 \pm 0.4)\%$ for Alq_3 and $\chi_S = (23 \pm 1)\%$ for MEH-PPV.

A direct experimental estimate of V_{sat} in Alq_3 can be obtained from Fig. 10 by extrapolating the EL efficiencies of Alq_3 to find the voltage at which the temperature dependence vanishes. The point at which the linear slopes of each temperature characteristic intersect in Fig. 10 is $V_{sat} = (15.1 \pm 1)$ V, which gives $\eta_f = 1.19\%$, and $\chi_S = (20 \pm 1)\%$ in Alq_3. The linearity of η_{EL} with voltage, its temperature dependence, and the intersection at V_{sat}, which is consistent with trap saturation, all strongly support the model of exciton formation described by Eq. (7).

Figure 11 shows that when measured at a sufficiently high current density such that V approaches V_{sat} (i.e., $J \approx 100$ mA/cm^2), η_{EL} approximately tracks η_{PL} over a large temperature range, indicating that $d(\gamma\chi_S)/dT = 0$ and $\gamma \approx 1$ for both Alq_3 and MEH-PPV. The singlet fractions for $\gamma \approx 1$ are shown in the insets as functions of temperature.

Finally, it is noted that even in the worst case, EL-specific losses contribute only a small correction to the measured value of the singlet fraction χ_S, and in both Alq_3 and MEH-PPV, $\chi_S \lesssim 25\%$. The best estimate for χ_S in Alq_3 uses V_{sat} derived from Fig. 10, and is $\chi_S = (20 \pm 1)\%$. Similarly, the best estimate for χ_S in MEH-PPV lies between the measured and worst-case values, i.e., $\chi_S = (20 \pm 4)\%$.

VI. DISCUSSION

Table I summarizes six experimental studies, including this work, of χ_S in small molecular and polymeric organic materials. The methods employed vary—Cao *et al.*[1] and Kim *et al.*[3] both employ absolute measurements of EL and PL efficiencies, while Wilson *et al.*[5] and our work use relative comparisons. Four independent measurements find $\chi_S \lesssim 0.25$ in molecular organic materials, but in previous work, χ_S in conjugated polymers was generally found to exceed 0.25. In addition to the methods reported in Table I, there are several measurements of χ_S that employ photoinduced absorption to calculate triplet densities.[34–36] Several of these measurements have also found $\chi_S > 0.25$.[35,36] High values of χ_S can possibly be interpreted in terms of the photophysical rates of Fig. 2. Tandon *et al.*[37] review theoretical estimates of k_S and k_T. They model these rates in polymers using parallel interacting chains and argue that electron correlations between delocalized states may account for $\chi_S > 0.25$.

The discrepancy between the present work and previous polymeric measurements that yield $\chi_S > 0.25$ requires comment. We now discuss these and the current measurements, together with the electron paramagnetic resonance (EPR) experiments of Wohlgenannt and co-workers[4,38] and Shinar and co-workers.[39,40] While all measurements of $\chi_S > 0.25$ require $k_S > k_T$, EPR experiments may provide a more direct probe of these rates.

A. Measurements of χ_S in small molecular materials

To maximize the OLED efficiency, it is desirable to harness all injected charges, either by developing systems with

TABLE I. Summary of various measurements of χ_S using EL/PL comparisons.

(a) Small molecular weight materials
  (i) Direct comparisons of EL to PL

Material	$\eta_c \eta_{PL}$ (%)	η_{EL} (%)	γ	χ_s	Ref.
Alq$_3$[a]	5.8	1.06	0.91 ± 0.05	0.20 ± 0.01	

  (ii) Phosphorescent techniques

Material	$\eta_{PL}^f / \eta_{PL}^p$	$\eta_{EL}^f / \eta_{EL}^p$	χ_s	Ref.
Pt monomer[b]	4.8	1.0	0.22 ± 0.01	5
CBP[c]		0.22	0.22 ± 0.02	30, 41
Alq$_3$[d]	2.7	0.56	0.22 ± 0.03	2

(b) Polymeric materials

  (i) Direct comparisons of EL to PL

Material	η_{PL} (%)	$\eta_c \eta_{PL}$ (%)	η_{EL} (%)	η_{EL} / η_c (%)	γ	χ_s	Ref.
OC1 C10-PPV[e]		8.5	4			>0.50	1
MEH-PPV[f]		8.5	1.3			>0.15	1
Green PPV[g]	33 ± 3		6 ± 0.5	23		$>0.35-0.45$	3
Orange PPV[h]	9 ± 1		1.8 ± 0.2	5.6		$>0.35-0.45$	3
MEH-PPV[i]		4.8	0.82		0.85 ± 0.15	0.20 ± 0.04	

  (ii) Phosphorescent techniques

Material	$\eta_{PL}^f / \eta_{PL}^p$	$\eta_{EL}^f / \eta_{EL}^p$	χ_s	Ref.
Pt polymer[j]	4.6	1.8	0.57 ± 0.04	5

[a]This work.

[b]The Pt-polymer in (b) and monomer are related. See Ref. 5 for chemical structures. The singlet fraction is determined from the ratios of fluorescent and phosphorescent efficiencies; see Eq. (10).

[c]Only the more accurate measurement in Ref. 30 has been quoted; see text. Electroluminescent efficiencies are quoted at $J = 1$ mA/cm^2.

[d]Fluorescent and phosphorescent efficiencies were obtained using fluorescent and phosphorescent guest molecules in an Alq$_3$ host.

[e]OC1 C10-PPV is [poly(2-(3,7-dimethyloctyloxy)-5-(2$'$ methoxy-1,4-phenylene vinylene). It was blended with 20% (2-(4-biphenyl)-5-(4-tert-butylphenyl)1,3,4-oxidiazole (Bu-PBD).

[f]MEH-PPV is poly[2-methoxy-5-(2-ethylhexyloxy)-1,4-phenylenevinylene].

[g]2-alkoxyphenyl-PPV-co-2,5-dialkoxy-PPV.

[h]2,5-dialkoxy-PPV.

[i]This work.

[j]The Pt polymer and monomer in (a) are related. See Ref. 5 for chemical structures. The singlet fraction is determined from the ratios of fluorescent and phosphorescent efficiencies; see Eq. (10). The singlet fraction $\chi_S = 0.57 \pm 0.04$ is obtained by averaging the results at different temperatures, not simply the room-temperature values of $\eta_{PL}^f / \eta_{PL}^p$ and $\eta_{EL}^f / \eta_{EL}^p$ given above.

$\chi_S \to 1$ or by also using phosphorescence from triplet states. Perhaps the first measurements of χ_S in an organic semiconductor used fluorescent and phosphorescent guest molecules to capture singlet and triplet excitons formed in an Alq$_3$ host.[2,27] The singlet ratio was estimated by identifying singlets by fluorescence and triplets by phosphorescence. Their ratio gave $\chi_S = (22 \pm 3)\%$ consistent with the current study.[2]

Subsequent refinements used phosphor-sensitized fluorescence, a technique that employs a fluorescent guest material mixed into a host.[41] To harness triplet excitons formed in the host, an additional sensitizing phosphorescent species is added to transfer triplet excitons to the singlet state of the guest with nearly 100% efficiency.[41] Thus only singlet excitons luminesce in the absence of the sensitizer, but both

triplets and singlets are detected when the sensitizer is included.

Figure 12 shows the quantum efficiency as a function of current density for two OLED's, one of which uses a sensitizer.[30] The host material is 4,4$'$-N,N$'$-dicarbazolyl-biphenyl (CBP), the fluorescent guest is DCM2, and the phosphorescent sensitizer is *fac* tris(2-phenylpyridine)iridium [Ir(ppy)$_3$]. The spin fraction is calculated from the ratio of efficiencies with and without the sensitizer to be $(22 \pm 2)\%$, independent of current density and electric field.[30] In both OLED's, luminescence is emitted from the guest fluorescent molecule, thereby eliminating errors due to the differing radiative efficiencies in comparisons of fluorescence and phosphorescence.[27] The technique may,
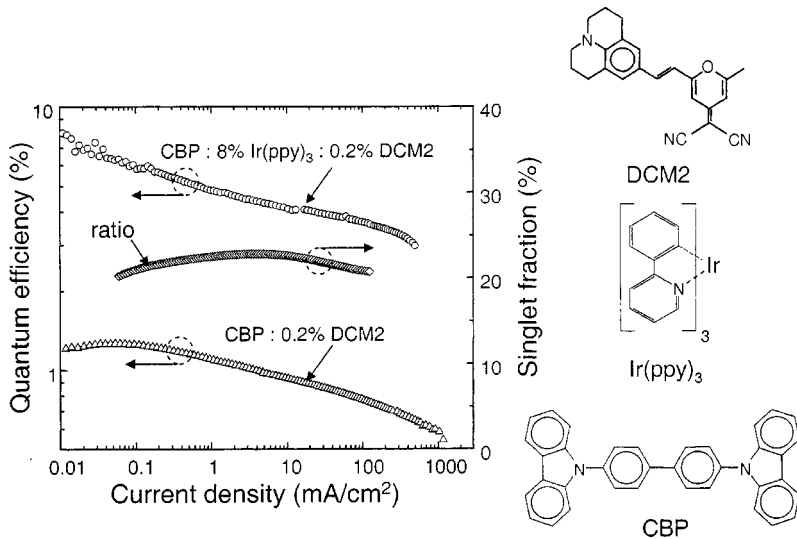
FIG. 12. The external quantum efficiencies of the fluorescent dye DCM2 with and without phosphorescent sensitization by tris-(2-phenylpyridine) iridium (Ir(ppy)$_3$). The host material is 4,4′-N,N′-dicarbazole-biphenyl (CBP). The chemical structures of the materials are shown in the inset. The ratio between sensitized and unsensitized emission gives $\chi_S = (22 \pm 2)\%$. Adapted from D'Andrade et al. (Ref. 30).

however, overestimate the singlet fraction if triplets form directly on the fluorescent guest rather than on the host or sensitizer. Thus the most accurate measurements[30] employ very low concentrations ($\approx 0.2\%$) of the fluorescent dye and high concentrations ($\approx 8\%$) of the phosphorescent sensitizer. Excitons may also form predominantly on the small molecular weight phosphorescent sensitizer when it is present at 8% in a host material.[42] Uncertainties in the exciton formation site prevent application of the small molecular weight phosphor sensitization technique to polymers. Together with the results from this work, and from Wilson et al. (discussed below), four independent measurements consistently find $0.20 < \chi_S < 0.22$ in small molecular weight materials.

B. Measurements of χ_S in polymeric materials comparing EL to PL

In contrast to small molecules, several measurements of conjugated polymers, using both absolute and relative techniques, find that $\chi_S > 0.25$. In their absolute measurements, Cao et al.[1] studied EL and PL from the same luminescent polymer film, thereby reducing systematic errors. Kim et al.[3] also compared EL and PL efficiencies, taking care to estimate microcavity effects within their EL devices so as to obtain a minimum value for χ_S. In measurements of neat films of OC1C10 (Table I) between temperatures of 290 and 360 K, Cao et al.[1] found $\gamma \chi_S \approx 0.25$. But in heterostructures with mixtures of OC1C10 and the electron-transporting small molecular weight material Bu-PBD, $\gamma \chi_S$ increased from 0.25 at room temperature to 0.5 at 360 K. The observed temperature dependence may be the result of variations in the EL-specific loss γ. However, our measurement of the temperature dependence of the EL efficiency of bilayer devices of MEH-PPV and the electron-transporting small molecular weight material BCP failed to repeat the effect; in fact the EL efficiency obtained here was found to have the opposite dependence on temperature from that of Cao.

In an alternate approach, Wilson and co-workers[5] use a Pt-containing polymer[43] and monomer with enhanced spin-orbit coupling that allows simultaneous measurement of fluorescence from singlets and phosphorescence from trip-

lets. While efficient ISC leads to almost 100% conversion into triplets, the fluorescence and phosphorescence intensities are comparable since the phosphorescence is weak and nonradiative processes dominate. The total photoluminescent efficiency at room temperature is 1.1% for the monomer and 0.24% for the polymer.[44] The singlet fraction is then inferred by comparing the ratio of fluorescence to phosphorescence in both EL and PL. The monomer and polymer moieties exhibit similar fluorescent and phosphorescent spectra, indicating that singlet and triplet excitons are confined to a single repeat unit along the chain. Differences in χ_S cannot therefore be attributed to delocalization that would typically accompany conjugation along the polymer backbone.[4,38,45,46]

Now, the ratio of fluorescence Φ_f to phosphorescence Φ_p in EL divided by PL gives, in terms of the rates in Fig. 2,

$$(\Phi_f/\Phi_p)_{EL}/(\Phi_f/\Phi_p)_{PL} = \frac{\chi_S}{b}\left(\frac{\eta_f}{\eta_p}\right)_{EL}\left(\frac{\eta_p}{\eta_f}\right)_{PL}, \quad (10)$$

where the fluorescent and phosphorescent efficiencies are $\eta_f = k_r^f/(k_r^f + k_{nr}^f + k_{ISC})$ and $\eta_p = k_r^p/(k_r^p + k_{nr}^p)$, respectively. The branching ratio b is

$$b = \frac{\chi_S k_{BS} + k_{S*}}{k_{S*} + k_{BS} + k_{ISC*}}, \quad (11)$$

where the mixing rate between singlet and triplet CT states is assumed to be high (k_{SL} large).

By this method, Wilson et al.[5] find that $\chi_S = (57 \pm 4)\%$ in their polymer and $\chi_S = (22 \pm 1)\%$ for the monomer. It is assumed that k_{ISC}, η_f, and η_p are the same in EL as they are in PL. It is also assumed that the branching ratio $b \approx 1$. When $b \approx 1$, $S^* \rightarrow S$ occurs with unit efficiency, so that optical excitation even well above the band edge[44] leads exclusively to S. This is a key assumption since χ_S is proportional to b [Eq. (10)]. CT states, however, provide additional pathways for energy relaxation. For example, excitation 0.5 eV above the band edge leads to a lowered quantum yield for fluorescence in a polysilane, but not in crystalline anthracene.[47] The value of b, then, may in fact be substantially below unity in polymers,[15,48] influencing measurements of χ_S. It is notable

that similar experiments employing phosphorescent iridium complexes grafted onto a polyfluorene backbone do not show $\chi_S > 0.25$.[49]

The possibility that the branching ratio is less than unity similarly affects the measurements by Cao *et al.*[1] and Kim *et al.*[3] given that the measured PL efficiency is proportional to b, so that $b < 1$ would result in an overestimate of χ_S. Measurements of χ_S that compare EL to PL efficiencies should therefore attempt to minimize or measure the rate of excited exciton dissociation into CT states. In this work, we minimize the effect of branching rates such as k_{ISC*} and k_{BS} by exciting the polymer at the edge of its absorption spectrum. In any case, our conclusion that $\chi_S < 25\%$ in MEH-PPV would not be changed by an underestimate of the PL efficiency.

One way to *ensure* correct accounting of the branching ratio in PL is to study polymers with high PL efficiencies, since, if $b\eta_f \rightarrow 1$, branching effects must be negligible. To date, measurements of $\chi_S > 25\%$ using comparisons of EL and PL have only been obtained in polymers with relatively low PL efficiencies as shown in Table I. Due to their high PL efficiencies, polyfluorenes seem especially suited to accurate measurements of χ_S.[50]

C. Spin-resonance measurements

In addition to measurements of χ_S based on a comparison of EL to PL efficiency, χ_S has been inferred from electron paramagnetic resonance (EPR) measurements. Wohlgenannt *et al.*[4,38] use photoabsorption detected magnetic resonance (PADMR) to obtain the ratio of k_S to k_T, and hence χ_S at any given k_{SL}, as a function of conjugation length in oligomeric and polymeric materials. This technique studies the change in polaron density in a material at low temperature (≈ 20 K) as it is swept through resonance. An applied magnetic field causes Zeeman splitting of the energies of the three triplet states, T_0, T_{-1}, and T_{+1}, of degenerate polaron pairs, which include CT states with $r > r_K$ (see Sec. I). Resonance is induced by an applied microwave field tuned to the Zeeman splitting, causing equalization of the populations of these three states. In the case of degenerate polaron pairs, but not in the case of excitons, the spin-zero triplet state T_0 is degenerate with the singlet state S_0 even under resonance, so the populations of the singlet and the three triplet states will be equalized.

In EPR therefore, T_0, T_{-1}, T_{+1}, and S_0 states each account for 25% of degenerate polaron pairs. From Fig. 2, because $k_{SL} \approx 0$ at low temperature, degenerate S_0 and T_0 polaron pairs form singlet and triplet excitons with rates, k_S and k_T, respectively, whereas T_{+1} and T_{-1} polaron pairs only form triplet excitons, with rate k_T. Population equalization through spin flipping in resonance allows polaron pairs initially formed in T_{+1} or T_{-1} combinations to cross to antiparallel combinations and eventually to form singlet excitons. Thus, under resonance conditions, either k_S or k_T can dominate exciton formation, and if one rate is larger than the other, the resonant rate of exciton formation will increase. Indeed, the decrease observed in the polaron absorption under resonance reflects a decrease in the polaron population,

and is consistent with $k_S \neq k_T$. Furthermore, the coincident decrease in the density of triplet excitons under resonance is consistent with $k_S > k_T$. Consequently, Wohlgenannt *et al.*[4,38] take $k_S > k_T$, and from changes in the polaron absorption under resonance calculate $1.7 < k_S/k_T < 5$ for a range of π-conjugated polymers and oligomers.

Now, the ionic character of singlet excitons may result in overlap with the initial polaron pair, leading to $k_S > k_T$.[4] In contrast, analyses of the magnetic-field dependence of photoconductivity in polymers suggest that $k_T > k_S$.[51] However, differences in exciton formation rates only influence the ultimate singlet fraction in EL if there is significant mixing of the immediate degenerate precursors to exciton formation, the degenerate CT states. From Fig. 2,

$$\chi_S = \frac{1 + k_{SL}/k_T}{4 + (k_{SL}/k_T)(1 + k_T/k_S)}. \qquad (12)$$

If $k_{SL} \gg k_S$, k_T, the singlet fraction reduces to[4,38,45]

$$\chi_S = \frac{1}{1 + 3k_T/k_S}. \qquad (13)$$

From Eq. (13) Wohlgenannt *et al.*,[4,38] infer $\chi_S > 0.25$ for a variety of polymers, and specifically $\chi_S = 47\%$ in MEH-PPV.

Electroluminescence-detected magnetic resonance (EL-DMR) is experimentally similar to PADMR except that EL instead of photoabsorption is the quantity examined under resonance. ELDMR can also be used to examine spin-dependent exciton formation. If PADMR results are attributable to spin-dependent recombination of degenerate polaron pairs, the decrease in triplet exciton and polaron populations observed under resonance should be associated with an increase in singlet excitons. The expected ELDMR signal is calculated as follows: in EL, 50% of charge-separated states are either S_0 or T_0. Outside of resonance, at low temperatures, and with an applied magnetic field causing Zeeman splitting, S_0 and T_0 are degenerate, and T_{+1} and T_{-1} are not degenerate nor are they mixed with S_0 and T_0. The resulting singlet fraction under EL outside of resonance is therefore $\chi_S = \frac{1}{2} k_S/(k_S + k_T)$. In resonance, EL from singlet excitons is proportional to $k_S/(k_S + 3k_T)$. Thus the expected ELDMR signal ΔEL is given by

$$\Delta\text{EL} = \frac{k_S/k_T - 1}{k_S/k_T + 3}. \qquad (14)$$

This change in EL intensity is expected to be 10–50% for the range of k_S/k_T values determined by PADMR.[4,38] However, the ELDMR signal of small molecular weight materials and polymers such as PPV actually shows a very slight increase[39] or even a decrease, both of magnitude $\Delta\text{EL} \approx 1 \times 10^{-4}$,[40] which clearly implies $k_S \approx k_T$. Negative PPV resonances may be partly attributed to a decrease in the conductivity of the devices under resonance conditions. The absence of large ELDMR signals in small molecular weight materials[52] and polymers strongly suggests that $k_S \approx k_T$ (and hence $\chi_S \approx 0.25$) in both types of materials. We note that while both EPR-based measurements of k_S and k_T, and EL/PL measurements are related to χ_S, they are not the same; the largest

k_S/k_T values are reported[4] for polymers that do not fluoresce, since the lowest-energy singlet state has A_g rather than B_u symmetry.

In summary, the CT and Frenkel states summarized in Fig. 1 and relaxation pathways in Fig. 2 are complicated and poorly quantified in most polymers. There are significant unresolved contradictions in the published measurements of χ_S that presently prevent a firm determination of the singlet fraction in polymeric materials, even in the specific case of MEH-PPV. In addition to varying results for χ_S, there are differences in the implied or reported temperature dependence[1,4,5] and electric-field dependence[1,5,34] of χ_S, and apparent differences between ELDMR and the interpretation of PADMR data. We have commented in this section on assumptions and approximations in reports of $\chi_S > 0.25$. We noted in Secs. IV and V some experimental considerations when measuring χ_S using the reverse bias technique, including a possible sensitivity to EL specific loss, which may be material dependent, and the requirement for efficient charge extraction, which also cannot be ensured in all cases.

VII. CONCLUSIONS

We use a simple reverse bias technique for measuring the photoluminescent (PL) efficiency of an organic light emitting device, and by comparing to the electroluminescent (EL) efficiency measured in the same geometry, find that the fraction of excitons formed as singlets in the electroluminescence of Alq_3 is $\chi_S = (20 \pm 1)\%$. This confirms other measurements showing that the exciton formation statistics in small molecular weight materials approximately follow the 25% spin-degeneracy statistical limit. MEH-PPV is found to have $\chi_S = (20 \pm 4)\%$, also consistent with the spin-degeneracy limit. This result in an archetypal conjugated polymer like MEH-PPV suggests that the singlet fraction may have a 25% limit in polymers generally, though the possibility that χ_S is material dependent cannot be ruled out.

Measurement of χ_S is motivated in part by its presumed relevance to highly efficient electroluminescent materials. In small molecular weight materials, the maximum observed EL quantum efficiency of fluorescent devices is 4–5%, but is ≈20% in small molecular weight phosphorescent devices.[7,53] Similar limits appear to hold for fluorescent polymer devices, i.e., external quantum efficiencies of ≪20%.[3,54] Given the high photoluminescent and outcoupling efficiencies of some polymers, it might be expected that measurements of $\chi_S > 25\%$ should be reflected in polymeric EL fluorescent quantum efficiencies that approach the $\eta_{EL} \approx 20\%$ observed in phosphorescent small molecular weight materials, although such efficiencies have not yet been demonstrated.

Thus in addition to the potential for providing insights into exciton formation, quantification of exciton formation statistics is critical to the full exploitation of organic electroluminescent technology. By harnessing triplets and singlets, phosphorescent OLED's exhibit efficiencies approximately four times that of molecular OLED's that fluoresce from singlets alone.[27] If, as is observed in this work, the formation statistics of excitons in polymeric semiconductors are similar to the statistics in small molecular weight mate-

rials, then it is clearly desirable to develop phosphorescent polymeric OLED's.

APPENDIX: TWO-TONE SYNCHRONOUS DETECTION FOR SPIN STATISTICS MEASUREMENTS

Field-induced dissociation of excitons in small molecular weight and polymeric materials typically requires the application of large ($>10^6$ V/cm) electric fields. However, application of these large fields may cause significant charge injection and leakage current in the OLED under study. Accurate determination of photoluminescent efficiencies requires the detection of the photocurrent component of the total current induced by photoexcitation and reverse bias. The two-tone synchronous measurement technique described in Fig. 3(b), isolates the small signal photocurrent component i_{ph} from leakage current i_{leak} by locking the total current signal to the optical chopping frequency. The total small signal current i is

$$i = i_{ph}(\omega_L, \omega_B) + i_{leak}(\omega_B), \tag{A1}$$

where ω_L and ω_B are the modulation angular frequencies of the photoexcitation and voltage bias, respectively. Since the leakage current is independent of optical excitation, detecting the component of the current at angular frequency ω_L isolates the photocurrent, i.e.,

$$\frac{1}{T} \int_L i \cos \omega_L t \, dt = i_{ph}, \tag{A2}$$

where T is the integration period, $T > 1/\omega_B$, $1/\omega_L$. The photocurrent i_{ph}, is

$$i_{ph} = \frac{1}{T} \int_T S(\omega_L t) f(V(t)) \cos \omega_L t \, dt. \tag{A3}$$

Here, $S(\omega_L t)$ [C/s] is the charge generation rate, assuming complete dissociation of all excitons; it is determined by the photoexcitation intensity and is chopped at angular frequency ω_L. Also, $f(V)$ is the electric field-induced dissociation probability of an exciton at an applied bias V. The voltage bias, and consequently the leakage current, is modulated at angular frequency ω_B. When $\omega_B \neq \omega_L$,

$$i_{ph} = \frac{\overline{f(V(t))}}{T} \int_T S(\omega_L t) \cos \omega_L t \, dt. \tag{A4}$$

The differential photoluminescence signal also contains two components: ΔP_d, the decrease in luminescence due to exciton dissociation, and ΔP_{ex}, due to random variations in the photoexcitation intensity. Furthermore, ΔP_{ex} causes random variations, δS, in the charge generation rate. Assuming that the average photoexcitation intensity is constant, detecting

the component of the total photoluminescence ΔP at angular frequency ω_B isolates the differential luminescence due to exciton dissociation, i.e.,

$$\frac{1}{T}\int_T \Delta P \cos \omega_B t\, dt = \Delta P_d. \tag{A5}$$

Specifically,

$$\Delta P_d = \frac{1}{T}\int_T \eta_C \eta_{PL}\frac{h\nu}{q}[S(\omega_L t)+\delta S(t)]f(V(t))\cos \omega_B t\, dt$$

$$= \eta_C \eta_{PL}\frac{h\nu}{q}\frac{\overline{S(\omega_L t)}}{T}\int_T f(V(t))\cos \omega_B t\, dt. \tag{A6}$$

Thus PL efficiencies measured using synchronous detection must be multiplied by the synchronous detection factor g:

$$\eta_C \eta_{PL} = g\left(\frac{q}{h\nu}\right)\frac{\Delta P_d}{i_{ph}}, \tag{A7}$$

where g is given by

$$g = \frac{\int_T S(\omega_L t)\cos \omega_L t\, dt}{\overline{S(\omega_L t)}}\frac{\overline{f(V(t))}}{\int_T f(V(t))\cos \omega_B t\, dt}. \tag{A8}$$

In our experiment, S may be approximated by a square wave with 50% duty cycle. Consequently,

$$\frac{\dfrac{1}{T}\int_T S(\omega_L t)\cos \omega_L t\, dt}{\overline{S(\omega_L t)}} = \frac{2}{\pi}. \tag{A9}$$

The function f is approximated by an Nth-order polynomial,

$$f(V) = \sum_{n=1}^{N} a_n V^n \tag{A10}$$

with coefficients a_n. Using the identity $\int_0^\pi \cos^{2n} x\, dx = (2n)!\pi/2^{2n}(n!)^2$ gives

$$g = \frac{2}{\pi}\left(\frac{2\displaystyle\sum_{n=1}^{N} a_n V^n \frac{(2n+2)!}{2^{2n+2}[(n+1)!]^2}}{\displaystyle\sum_{n=1}^{N} a_n V^n \frac{(2n)!}{2^{2n}[n!]^2}} - 1\right)^{-1}. \tag{A11}$$
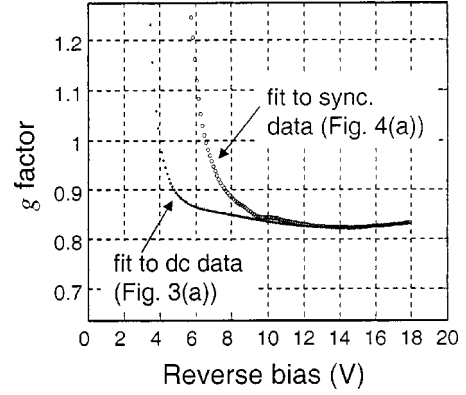

FIG. 13. Numerical evaluations of Appendix Eq. (A8), using fits to experimental data for the electric-field-induced dissociation probability f. These curves are used to determine the synchronous detection factor g in MEH-PPV. It is observed that both dc and synchronously detected measurements of f yield the same values of g at large values of reverse bias. A value of $g = 0.82 \pm 0.03$ is then calculated from data in Figs. 5(a) and 6(a).

Thus exact determination of the detection factor g, and hence the out-coupled PL efficiency $\eta_C \eta_{PL}$, requires the form of the nonlinear function $f(V)$. Ideally, the polynomial coefficients a_n should be obtained from a Taylor series expansion of experimental measurements of f. In Fig. 13 we show g obtained from experimental data. However, examination of Eq. (A11) demonstrates the presence of some limits.

If f is linearly related to applied voltage, then

$$g = \frac{4}{\pi}. \tag{A12}$$

This limit holds in Alq$_3$ above a threshold in the applied electric field.

If f is a nonlinear function such that $a_n \neq 0$ for large n, then

$$\lim_{V\to\infty} g = \frac{2}{\pi}. \tag{A13}$$

In general,

$$g = \frac{1}{\pi}(3 \pm 1). \tag{A14}$$

giving, in the worst case, a 33% error in the determination of $\eta_C \eta_{PL}$.

*Author to whom correspondence should be addressed. Electronic address: baldo@mit.edu

[1] Y. Cao, I. Parker, G. Yu, Z. C. , and A. Heeger, Nature (London) **397**, 414 (1999).

[2] M. A. Baldo, D. F. O'Brien, M. E. Thompson, and S. R. Forrest, Phys. Rev. B **60**, 14 422 (1999).

[3] J.-S. Kim, P. K. H. Ho, N. C. Greenham, and R. H. Friend, J. Appl. Phys. **88**, 1073 (2000).

[4] M. Wohlgenannt, K. Tandon, S. Mazumdar, S. Ramasesha, and Z. V. Vardeny, Nature (London) **409**, 494 (2001).

[5] J. S. Wilson, A. S. Dhoot, A. J. A. B. Seeley, M. S. Khan, A. Köhler, and R. H. Friend, Nature (London) **413**, 828 (2001).

[6] M. Wohlgenannt and Z. V. Vardeny, Synth. Met. **125**, 55 (2002).

[7] C. Adachi, M. A. Baldo, M. E. Thompson, and S. R. Forrest, J. Appl. Phys. **90**, 5048 (2001).

[8] A. P. Monkman, H. D. Burrows, L. J. Hartwell, L. E. Horsburgh, I. Hamblett, and S. Navaratnam, Phys. Rev. Lett. **86**, 1358 (2001).

[9] J. B. Birks, *Organic Molecular Photophysics* (J. Wiley, London, 1975).

[10] M. Pope and C. Swenberg, *Electronic Processes in Organic Crystals* (Oxford University Press, Oxford, 1982).

[11] D. S. McClure, J. Chem. Phys. **20**, 682 (1952).

[12] R. C. Hughes and Z. G. Soos, Chem. Phys. **63**, 1122 (1975).

[13] M. I. Khan, G. C. Bazan, and Z. D. Popovic, Chem. Phys. Lett. **298**, 309 (1998).

[14] W. Stampor, J. Kalinowski, P. D. Marco, and V. Fattori, Appl. Phys. Lett. **70**, 1935 (1997).

[15] N. T. Harrison, G. R. Hayes, R. T. Phillips, and R. H. Friend, Phys. Rev. Lett. **77**, 1881 (1996).

[16] M. Segal and M. A. Baldo, Organic Electronics (to be published).

[17] Results were confirmed using material from two suppliers: American Dye Source, 555 Morgan Blvd., Baie D'Urfe, Quebec, Canada H9X 3T6, and H. W. Sands, 1080 E. Indiantown Rd., Suite 206, Jupiter, FL 33477. The molecular weights of each polymer were reported to be 10^6 and 35 000, respectively.

[18] D. Z. Garbuzov, V. Bulovic, P. E. Burrows, and S. R. Forrest, Chem. Phys. Lett. **249**, 433 (1996).

[19] H. Mattoussi, H. Murata, C. D. Merritt, Y. Iizumi, J. Kido, and Z. H. Kafafi, J. Appl. Phys. **86**, 2642 (1999).

[20] V. Bulovic, V. B. Khalfin, G. Gu, P. E. Burrows, D. Z. Garbuzov, and S. R. Forrest, Phys. Rev. B **58**, 3730 (1998).

[21] N. Greenham, I. Samuel, G. Hayes, R. Philips, Y. Kessener, S. Moratti, A. Holmes, and R. Friend, Chem. Phys. Lett. **241**, 89 (1995).

[22] P. F. van Hutten, V. V. Krasnikov, and G. Hadziioannou, Synth. Met. **122**, 83 (2001).

[23] I. G. Hill and A. Kahn, J. Appl. Phys. **86**, 4515 (1999).

[24] P. Peumans and S. Forrest, Appl. Phys. Lett. **79**, 126 (2001).

[25] M. A. Baldo and S. R. Forrest, Phys. Rev. B **64**, 085201 (2001).

[26] R. R. Chance, A. Prock, and R. Sibley, Adv. Chem. Phys. **37**, 1 (1978).

[27] M. A. Baldo, D. F. O'Brien, Y. You, A. Shoustikov, S. Sibley, M. E. Thompson, and S. R. Forrest, Nature (London) **395**, 151 (1998).

[28] M. A. Baldo, C. Adachi, and S. R. Forrest, Phys. Rev. B **62**, 10 967 (2000).

[29] P. E. Burrows, Z. Shen, V. Bulovic, D. M. McCarty, S. R. Forrest, J. A. Cronin, and M. E. Thompson, J. Appl. Phys. **79**, 7991 (1996).

[30] B. W. D'Andrade, M. A. Baldo, C. Adachi, J. Brooks, M. E. Thompson, and S. R. Forrest, Appl. Phys. Lett. **79**, 1045 (2001).

[31] M. A. Baldo, M. E. Thompson, and S. R. Forrest, Pure Appl. Chem. **71**, 2095 (1999).

[32] M. A. Baldo, R. J. Holmes, and S. R. Forrest, Phys. Rev. B **66**, 035321 (2002).

[33] T. Förster, Discuss. Faraday Soc. **27**, 7 (1959).

[34] L. C. Lin, H. F. Meng, J. T. Shy, S. F. Horng, L. S. Yu, C. H. Chen, H. H. Liaw, C. C. Huang, K. Y. Peng, and S. A. Chen, Phys. Rev. Lett. **90**, 036601 (2003).

[35] A. S. Dhoot, D. S. Ginger, D. Beljonne, Z. Shuai, and N. C. Greenham, Chem. Phys. Lett. **360**, 195 (2002).

[36] A. S. Dhoot and N. C. Greenham, Adv. Mater. (Weinheim, Ger.) **14**, 1834 (2002).

[37] K. Tandon, S. Ramasesha, and S. Mazumdar, Phys. Rev. B **67**, 045109 (2003).

[38] M. Wohlgenannt, X. M. Jiang, Z. V. Vardeny, and R. A. J. Janssen, Phys. Rev. Lett. **88**, 197401 (2002).

[39] N. C. Greenham, J. Shinar, J. Partee, P. A. Lane, O. Amir, F. Lu, and R. H. Friend, Phys. Rev. B **53**, 13 528 (1996).

[40] L. S. Swanson, J. Shinar, A. R. Brown, D. D. C. Bradley, R. H. Friend, P. L. Burn, A. Kraft, and A. B. Holmes, Phys. Rev. B **46**, 15 072 (1992).

[41] M. A. Baldo, M. E. Thompson, and S. R. Forrest, Nature (London) **403**, 750 (2000).

[42] M. A. Baldo and S. R. Forrest, Phys. Rev. B **62**, 10 958 (2000).

[43] A. Köhler, M. Younus, M. R. A. Al-Mandhary, P. R. Raithby, M. S. Khan, and R. H. Friend, Synth. Met. **101**, 246 (1997).

[44] J. S. Wilson, N. Chawdhury, M. R. A. Al-Mandhary, M. Younus, M. S. Khan, P. R. Raithby, A. Köhler, and R. H. Friend, J. Am. Chem. Soc. **123**, 9412 (2001).

[45] Z. Shuai, D. Beljonne, R. J. Silbey, and J. L. Bredas, Phys. Rev. Lett. **84**, 131 (2000).

[46] D. Beljonne, Z. Shuai, J. Cornil, J. P. Calbert, and J. L. Brédas, J. Photochem. Photobiol., A **144**, 57 (2001).

[47] R. G. Kepler, J. M. Zeigler, L. A. Harrah, and S. R. Kurtz, Phys. Rev. B **35**, 2818 (1987).

[48] G. J. Denton, N. Tessler, N. T. Harrison, and R. H. Friend, Phys. Rev. Lett. **78**, 733 (1997).

[49] X. Chen, J.-L. Liao, Y. Liang, M. O. Ahmed, H.-E. Tseng, and S.-A. Chen, J. Am. Chem. Soc. **125**, 636 (2003).

[50] A. W. Grice, D. D. C. Bradley, M. T. Bernius, M. Inbasekaran, W. W. Wu, and E. P. Woo, Appl. Phys. Lett. **73**, 629 (1998).

[51] E. L. Frankevich, A. A. Lymarev, I. Sokolik, F. E. Karasz, S. Blumstengel, R. H. Baughman, and H. H. Hörhold, Phys. Rev. B **46**, 9320 (1992).

[52] J. Shinar (unpublished).

[53] M. Ikai, S. Tokito, Y. Sakamoto, T. Suzuki, and Y. Taga, Appl. Phys. Lett. **79**, 156 (2001).

[54] R. H. Friend, R. W. Gymer, A. B. Holmes, J. H. Burroughes, R. N. Marks, C. Taliani, D. D. C. Bradley, D. A. Dos Santos, J. L. Bredas, M. Logdlund, and W. R. Salaneck, Nature (London) **397**, 121 (1999).